ISSN: 1983 7402 ITA, 29 a 30 SET 2020

Photonic-Assisted Microwave Frequency Measurement Towards for Cognitive Radio

Robson R. Carreira[1,2], Joaquim J. Barroso[1], José E. B. Oliveira[1], André P. Gonçalves[1,2] and Alessandro R. Santos[1,2]
[1]Instituto Tecnológico de Aeronáutica, São José dos Campos, SP - Brazil
[2]Centro de Coordenação de Estudos da Marinha em São Paulo, São Paulo, SP - Brazil

***Abstract*—Cognitive RF systems can be seen through a OODA (Observe, Orient, Decide and Act) loop and Electronic warfare (EW) can be used in some of these stages, namely the Observe and the Act. Instantaneous Microwave Frequency Measurement (IFM) systems can contribute with cognitive RF technology taking the real world to the data world. In a OODA loop, IFM can be arranged as in the Observe stage. Here we propose an IFM device that allows the adjustment of the directional couplers coupling coefficients, optical fiber lengths, modulation index and modulation formats, what makes the system tunable. The semi-analytical model result shows good agreement with the simulation, achieving frequency differences of 130 MHz and 210 MHz for the lowest and highest amplitude comparison function (ACF) values, respectively.**

***Keywords*—electronic warefare, instantaneous frequency measurement, amplitude comparison function**

I. Introduction

Cognitive radio technology has been considered a way to perform a spectrum management due to its ability in learn, infer and react to the environment. Cognitive RF systems can be described as an OODA loop (Observe, Orient, Decide and Act) as showed in Fig. 1. First, the electromagnetic spectrum is observed through a sensor. Then, the information is processed and oriented, enabling a decision making. Finally, it becomes an act when configuring the transceiver in a proper way [1].

Electronic warfare (EW) is the only discipline operating in the electromagnetic spectrum in the Observe and the Act stages [1]. An available frequency operating range has become scarce due to the wireless devices and systems electromagnetic environment increasing demand. Therefore, a spectrum management implementation can make RF systems work in a complex electromagnetic environment in a more effective way [1]. In this sense, instantaneous microwave frequency measurement (IFM) systems can contribute with cognitive RF technology taking the real world to the data world. In a OODA loop, IFM can be arranged as in the Observe stage.

IFM has been used in EW applications, specially electronic support measures (ESM), for over sixty years [2]. Recently, microwave EW industry reached the technology maturity and, thenceforth, applications based on microwave-photonics (MP) have emerged, the so called photonic-assisted IFM [2]. Nowadays, authors have proposed several architectures aiming IFM applications [3]–[6].

Here, we propose a functional block for electromagnetic sensing in order to provide data acquisition for a radio cognitive system. This approach allows representation in both time and frequency domains besides offering more flexibility to set up a greater number of parameters, namely directional couplers (DC) coefficients, high modulation indexes, and amplitude comparison function (ACF) for double-sideband (DSB) and single-sideband (SSB) modulation formats. This tunable system can be overviewed by a semi-analytical model specifically developed that includes higher order lateral bands, enabling instantaneous ACF ratios for spectral components of orders different than unity [7].

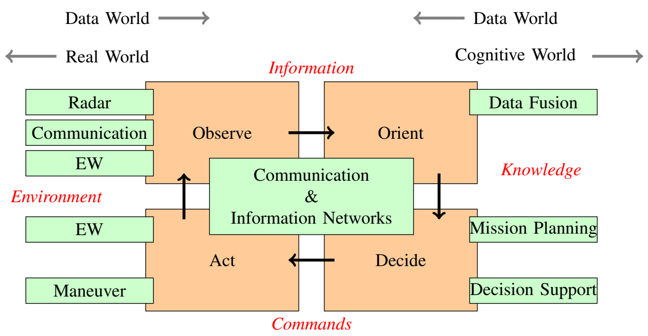

Fig. 1. Cognitive RF systems viewed as an OODA loop [1]. The proposed IFM system is included in the EW block connecting the real world to the data world feeding the Observe block.

II. Operation Principle

A generic photonic-assisted IFM system architecture can be represented by the block diagram shown in the Fig. 2. It consists of a light source, an electrical-to-optical conversion module, a photonic processing module, an optical-to-electrical conversion module, and a post-processing module.

The functional block diagram proposed is shown in Fig. 3. When correlating it with the generic photonic-assisted IFM system architecture in Fig. 2, the laser is the optical source, the dual-output dual-drive Mach-Zehnder modulator (DD-MZM) is the electrical-to-optical conversion module, and the two distinct standard single-mode fiber (SSMF), with lengths L_1 and L_2, are the photonic processing module, as they perform the desirable chromatic dispersion (CD) effect, which enable the notch regions inherent to the ACF parameter. The two PIN photodetectors (PD) are the optical-to-electrical conversion module. The DD-MZM internal structure is represented by two directional couplers (DC) with arbitrary coupling coef-

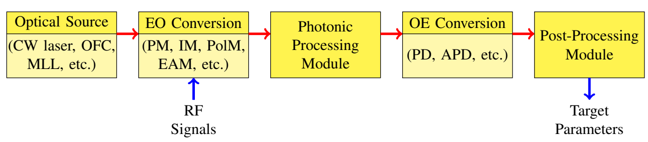

Fig. 2. Generic photonic-assisted IFM system architecture block diagram [8].

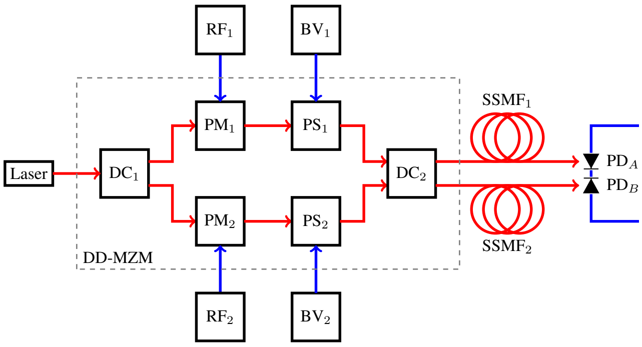

Fig. 3. Functional block diagram of a typical IFM system. PM means phase modulator, PS is phase shifter, DC is directional coupler, SSMF is standard single-mode fiber, PD is photodetector, BV is bias voltage and RF denotes to radio frequency signal [7].

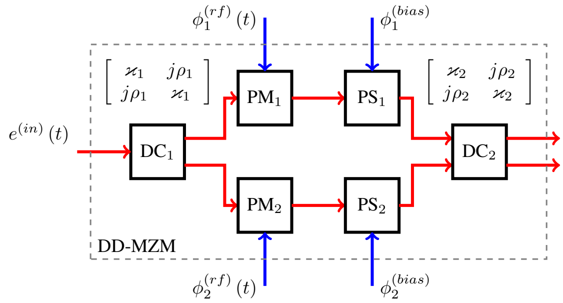

Fig. 4. Schematic representation of a dual-output DD-MZM in terms of a functional block diagram with coupling coefficients scattering matrices. Electric fields $e_1^{(out)}(t)$ and $e_2^{(out)}(t)$ feed distinct optical fiber paths [7].

ficients – the first DC (DC$_1$) works as an optical splitter –, two phase modulators (PM), and two phase shifters (PS). The PM can be fed, independently, by RF signals, RF$_1$ and RF$_2$, and the PS by distinct DC bias voltages, BV$_1$ and BV$_2$. This block diagram gives a global picture of a generalized IFM system aiming to obtain a power-to-frequency relationship. In other words, the ACF. To be effective, this parameter should be represented by a sharp curve as function of the input microwave frequency [9].

III. Formulation of the Problem

For a better understanding of the proposed device, Fig. 4 shows an enlarged view of the dual-output DD-MZM. In the DC$_1$ block, $e^{(in)}(t) = E^{(in)} \cos(\omega_o t + \phi_o)$ is splitted according to the coupling coefficients $\varkappa_1$ and ρ_1. Usually, a 3 dB ratio is used, but here we propose the possibility of using arbitrary values of these coefficients, obeying the condition $\varkappa_i^2 + \rho_i^2 = 1$, with $i = 1; 2$, by calculating the DC$_i$ scattering matrix [10]. These two new optical electric fields are modulated in the PM blocks by RF signals and biased in the PS blocks. These electric fields are recombined in the DC$_2$ block according to its scattering matrix with coupling coefficients $\varkappa_2$ and ρ_2. In the proposed scheme, all of these blocks are parameterizable.

It is emphasized that the dual-output DD-MZM permits some modulation formats, e.g., double-sideband (DSB), single-sideband (SSB) and double-sideband supressed carrier (DSB-SC). The SSB can be split in lower-sideband (LSB) and upper-sideband (USB) in the outputs 1 and 2, respectively. In this paper, only DSB and SSB are used due to DSB-SC format to provide one output with odd order components and the other one with the even orders. This special characteristic will be subject of a specific work.

These electric field outputs, $e_1^{(out)}(t)$ and $e_2^{(out)}(t)$, which obey the principle of energy conservation, feed distinct SSMF paths. Assuming $\overline{E}^{(in)} = E^{(in)} \mathrm{e}^{j\phi_o}$ as the complex optical electric field input envelope, and RF signals with the same frequency and amplitude feeding the PM$_1$ and PM$_2$, the DC$_2$ output complex envelopes can be given by [7]:

$$\overline{E}_1^{(out)} = \Gamma \overline{E}^{(in)} \sum_{n=-\infty}^{+\infty} a_n^{(1)} J_n(m)\, \mathrm{e}^{jn\omega_{rf}t} \tag{1a}$$

$$\overline{E}_2^{(out)} = j\Gamma \overline{E}^{(in)} \sum_{n=-\infty}^{+\infty} a_n^{(2)} J_n(m)\, \mathrm{e}^{jn\omega_{rf}t} \tag{1b}$$

where Γ is the link power insertion loss, J_n is the n-th order Bessel function of the first kind, $m = \pi V_{rf}/V_\pi$ is the modulation index, being V_{rf} the RF signal amplitude and V_π the DD-MZM half-wave voltage, and:

$$a_n^{(1)} = \varkappa_1\varkappa_2\, \mathrm{e}^{j\left(n\phi_1^{(0)} + \phi_1^{(bias)}\right)} - \rho_1\rho_2\, \mathrm{e}^{j\left(n\phi_2^{(0)} + \phi_2^{(bias)}\right)} \tag{2a}$$

$$a_n^{(2)} = \varkappa_1\rho_2\, \mathrm{e}^{j\left(n\phi_1^{(0)} + \phi_1^{(bias)}\right)} + \varkappa_2\rho_1\, \mathrm{e}^{j\left(n\phi_2^{(0)} + \phi_2^{(bias)}\right)} \tag{2b}$$

where $\phi_i^{(0)}$ is the PM$_i$ RF signal initial phase and $\phi_i^{(bias)}$ is the DC bias phase shift inserted by the PS$_i$.

The output signals travel through optical fiber paths with lengths L$_1$ and L$_2$ and then are detected by PD$_A$ and PD$_B$. At this point the CD and attenuation effects of each fiber path are take into account. Thus, the complex envelopes incident in PD$_A$ and PD$_B$ are:

$$\overline{E}_A = \overline{E}_1^{(out)}\, \mathrm{e}^{-\gamma(\omega_o + n\omega_{rf})L_1} \tag{3a}$$

$$\overline{E}_B = \overline{E}_2^{(out)}\, \mathrm{e}^{-\gamma(\omega_o + n\omega_{rf})L_2} \tag{3b}$$

where γ is the fiber-optic propagation constant. The photocurrent in each PD is given by:

$$I_{A,B}(t) = \frac{\Re_{A;B}}{2\eta} \left\langle |e_{A,B}^{(out)}(t)|^2 \right\rangle \xi \tag{4}$$

where the bracketed term means the time average of $|e_{A,B}^{(out)}(t)|^2$ over an optical cycle, A, B refers to each PD, $\Re_{A;B}$ are the PD responsivities, ξ is the PD effective cross sections and η the optical wave impedance. Expanding γ in Taylor series and substituting (3) in (4), one takes:

$$\begin{aligned} I_A(t) = {} & \Re_A \Gamma^2 P^{(in)}\, \mathrm{e}^{-2\alpha_1 L_1} \sum_{n=-\infty}^{+\infty} j^n\, \mathrm{e}^{jn\omega_{rf}t} \times \\ & \times \Big\{ \varkappa_1^2\varkappa_2^2\, \mathrm{e}^{jn\Delta\phi_{rf}}\, J_n[-2m\sin(\Phi_1)] + \\ & + \rho_1^2\rho_2^2 J_n[-2m\sin(\Phi_1)] + \\ & - \varkappa_1\varkappa_2\rho_1\rho_2\, \mathrm{e}^{j\left(\frac{n\Delta\phi_{rf}}{2} + \Delta\phi_{bias}\right)}\, J_n\left[2m\sin\left(\tfrac{\Delta\phi_{rf}}{2} - \Phi_1\right)\right] + \\ & - \varkappa_1\varkappa_2\rho_1\rho_2\, \mathrm{e}^{j\left(\frac{n\Delta\phi_{rf}}{2} - \Delta\phi_{bias}\right)}\, J_n\left[-2m\sin\left(\tfrac{\Delta\phi_{rf}}{2} + \Phi_1\right)\right] \Big\} \end{aligned} \tag{5a}$$

$$\begin{aligned} I_B(t) = {} & \Re_B \Gamma^2 P^{(in)} \, \mathrm{e}^{-2\alpha_2 L_2} \sum_{n=-\infty}^{+\infty} j^n \, \mathrm{e}^{jn\omega_{rf}t} \times \\ & \times \left\{ \varkappa_1^2 \rho_2^2 \, \mathrm{e}^{jn\Delta\phi_{rf}} \, J_n[-2m \sin(\Phi_2)] + \right. \\ & + \varkappa_2^2 \rho_1^2 J_n[-2m \sin(\Phi_2)] + \\ & + \varkappa_1 \varkappa_2 \rho_1 \rho_2 \, \mathrm{e}^{j\left(\frac{n\Delta\phi_{rf}}{2} + \Delta\phi_{bias}\right)} \, J_n\left[2m \sin\left(\tfrac{\Delta\phi_{rf}}{2} - \Phi_2\right)\right] + \\ & \left. + \varkappa_1 \varkappa_2 \rho_1 \rho_2 \, \mathrm{e}^{j\left(\frac{n\Delta\phi_{rf}}{2} - \Delta\phi_{bias}\right)} \, J_n\left[-2m \sin\left(\tfrac{\Delta\phi_{rf}}{2} + \Phi_2\right)\right] \right\} \end{aligned} \tag{5b}$$

where $\Delta\phi_{bias}$ is the DD-MZM DC bias phase shift, $\Delta\phi_{rf}$ is the RF phase change set in a hybrid, $\alpha_{1;2}$ are the optical fiber attenuations, $\Phi_{1;2} = \beta_2 \omega_{rf}^2 n L_{1;2}/2$, $\beta_2 = -D_{1;2}\lambda_o^2/2\pi c$ is the second-order dispersion coefficient, $D_{1;2}$ are the fiber dispersion parameters, λ_o is the laser wavelength and c is the speed of light in vacuum. The Graf's addition theorem was used to calculate the current waveform in each PD, enabling a model not limited to small signals, thus allowing the consideration of high modulation indexes [11]. Likewise, the ACF can be obtained for DSB and SSB modulation formats thanks to the use of a dual-output DD-MZM, what makes the system tunable. The semi-analytical model developed also includes higher order lateral bands, enabling ACF ratios for spectral components of orders different than unity.

To allow a proper discussion, the DD-MZM is setted for a SSB modulation format ($\Delta\phi_{bias} = \pi/2$ and $\Delta\phi_{rf} = \pi/2$), the DC coupling coefficients are setted for 3 dB and the first harmonic component is selected ($n = 1$). Therefore, from (5) one can obtain the instantaneous RF power output $P_{rf}^{(A;B)}(t) = I_{A;B}(t)^2 Z_{A;B}$ for each PD, where $Z_{A;B}$ is the $\mathrm{PD}_{A;B}$ impedance:

$$\begin{aligned} P_A(t) = A_A^2 \left[B_A^2 + C_A^2 + \left(B_A^2 - C_A^2\right) \sin(2\omega t) + \right. \\ \left. + \, 2 B_A C_A \cos(2\omega t) \right] \end{aligned} \tag{6a}$$

$$\begin{aligned} P_B(t) = A_B^2 \left[B_B^2 + C_B^2 + \left(B_B^2 - C_B^2\right) \sin(2\omega t) + \right. \\ \left. - \, 2 B_B C_B \cos(2\omega t) \right] \end{aligned} \tag{6b}$$

where:

$$A_{A;B} = \frac{\Re_{A;B}}{4} \Gamma^2 P^{(in)} \, \mathrm{e}^{-2\alpha_{1;2} L_{1;2}} \, Z_{A;B} \tag{7a}$$

$$B_{A;B} = J_1 \left[2m \sin(\Phi_{1;2})\right] \tag{7b}$$

$$\begin{aligned} C_{A;B} = \frac{\sqrt{2}}{2} \left\{ J_1 \left[m\sqrt{2} \left(\cos\Phi_{1;2} - \sin\Phi_{1;2}\right) \right] + \right. \\ \left. + J_1 \left[m\sqrt{2} \left(\cos\Phi_{1;2} + \sin\Phi_{1;2}\right) \right] \right\} \end{aligned} \tag{7c}$$

Equations (6) show terms related to active and reactive power, cosine and sine, respectively, that will be discussed in future works. Here we are interested in the instantaneous ACF which is defined by the ratio between the RF power obtained in PD_A and PD_B [4], [12]. Thus, assuming the same fiber lengths ($L_1 = L_2$), dispersion parameters ($D_1 = D_2$), PD responsivities ($\Re_A = \Re_B$) and impedances ($Z_A = Z_B$), in a instant $t = \pi/2\omega_{rf}$, one takes:

$$ACF = \frac{P_A(t)}{P_B(t)} = \left(\frac{B - C}{B + C}\right)^2 \tag{8}$$

Equation (8), as far as we know, is not represented in the literature. It allows to reproduce previously published results and provides new ones, e.g., high modulation indexes influence.

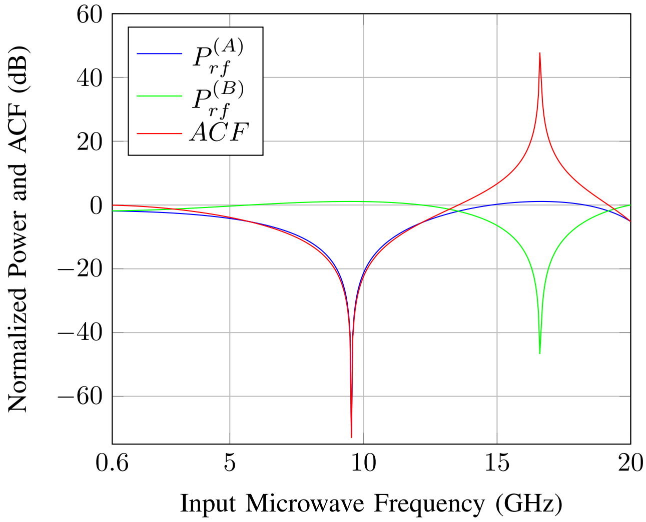

Fig. 5. PD_A and PD_B RF power, normalized with respect to the maximum value of $P_{rf}^{(B)}$, and ACF for modulation format SSB, modulation index $m = 0.2$, optical fiber path 1 $L_1 = 20$ km, optical fiber path 2 $L_2 = 20$ km and DC_1 and DC_2 coupling coefficients setted with 3 dB.

IV. Numerical and Simulation Results

For the numerical analysis, it is assumed $m = 0.2$ (low modulation index), $L = 20$ km, $D = 17$ ps/km.nm and $\lambda_o = 1550$ nm in (8). Fig. 5 shows PD_A and PD_B RF power outputs, normalized with respect to the maximum value of $P_{rf}^{(B)}$, and ACF. Note that, from (8), $P_{rf}^{(A)}(t)$ and $P_{rf}^{(B)}(t)$ are the active powers in the instant $t = \pi/2\omega_{rf}$. Furthermore, Fig. 5 reproduces [5] even with both PM fed by RF signals.

For the simulation analysis, the Optisystem 17.0 is setted with the same parameter values as the numerical analysis. Fig. 6 presents both the numerical and simulation results, showing good agreement. The lowest ACF value is -67.99 dB in 9.69 GHz for the simulation while is -64.14 dB in 9.56 GHz for the numerical. It represents an ACF difference of 3.85 dB and a frequency difference of 130 MHz. The highest ACF value is 52.35 dB in 16.82 GHz for the simulation while is 54.93 dB in 16.61 GHz for the numerical. It represents a difference in ACF of 2.58 dB and in frequency of 210 MHz.

As discussed in the previous section, (5) allows flexibility to vary other parameters, e.g., DC coupling coefficients, fiber length, modulation index and modulation formats. In this work we are interested in a SSB approach with low modulation index, same fiber length and 3 dB DC coupling coefficients aiming the comparation between the numerical and simulation with previous published results. The variation of these other parameters and the other possible contributions to cognitive radio will be subject of future works.

V. Conclusion

In this work we discussed a photonic-assisted microwave frequency measurement towards for cognitive radio. The proposed device permits some parameter adjustments, namely, DC coupling coefficients, fiber length, modulation index and modulation formats, what makes the system tunable. As far as our knowledge under the subject, this work brings a novel and complete semi-analytical model not clearly presented in the literature. It reproduces previous published results besides the good agreement with the simulation result. The frequency

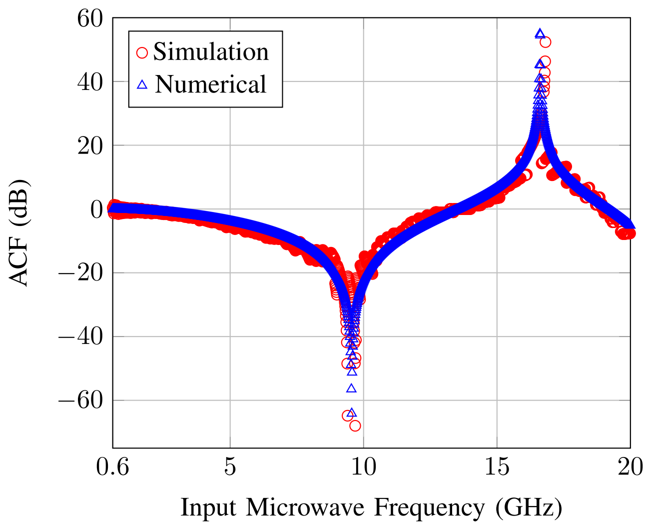

Fig. 6. Simulation and numerical results for ACF. The lowest value difference are 3.85 dB for the ACF and 130 MHz for the frequency. The highest value difference are 2.58 dB for the ACF and 210 MHz for the frequency.

differences between the numerical and simulation results are 130 MHz and 210 MHz for the lowest and highest ACF values, respectively. The authors emphasize that this is not a final work, but part of an ongoing doctorate. It is advancing towards to incorporating coherent detection in the scheme and also optical fiber nonlinearities.

Acknowledgment

The authors would like to thanks the Brazilian Navy and the Brazilian Air Force for the support.

References

[1] D. Zhu and S. Pan, "Broadband cognitive radio enabled by photonics," *Journal of Lightwave Technology*, vol. 38, no. 12, pp. 3076–3088, Jun 2020.

[2] P. W. East, "Fifty years of instantaneous frequency measurement," *IET Radar, Sonar & Navigation*, vol. 6, no. 2, p. 112, Feb. 2012.

[3] Y. Li, L. Pei, J. Li, J. Zheng, Y. Wang, J. Yuan, and Y. Tang, "Instantaneous microwave frequency measurement with improved resolution," *Optics Communications*, vol. 354, pp. 140–147, Nov. 2015.

[4] J. Zhou, S. Fu, S. Aditya, P. P. Shum, and C. Lin, "Instantaneous microwave frequency measurement using photonic technique," *IEEE Photonics Technology Letters*, vol. 21, no. 15, pp. 1069–1071, Aug. 2009.

[5] J. Li, S. Fu, K. Xu, J. Q. Zhou, P. Shum, J. Wu, and J. Lin, "Photonic-assisted microwave frequency measurement with higher resolution and tunable range," *Optics Letters*, vol. 34, no. 6, p. 743, Mar. 2009.

[6] L. A. Bui, "Recent advances in microwave photonics instantaneous frequency measurements," *Progress in Quantum Electronics*, vol. 69, p. 100237, Jan 2020.

[7] R. R. Carreira, J. J. Barroso, J. E. B. Oliveira, A. P. Gonçalves, A. R. Santos, O. L. Coutinho, V. R. Almeida, and C. S. Martins, "Generalized analysis of a tunable range photonic-assisted instantaneous frequency measurement of microwave signals," 2020, Manuscript submitted for publication.

[8] X. Zou, B. Lu, W. Pan, L. Yan, A. Stöhr, and J. Yao, "Photonics for microwave measurements," *Laser & Photonics Reviews*, vol. 10, no. 5, pp. 711–734, 2016.

[9] X. Zou, H. Chi, and J. Yao, "Microwave frequency measurement based on optical power monitoring using a complementary optical filter pair," *IEEE Transactions on Microwave Theory and Techniques*, vol. 57, no. 2, pp. 505–511, Feb. 2009.

[10] R. H. Rediker and F. J. Leonbercer, "Analysis of integrated-optics near 3 dB coupler and mach-zehnder interferometric modulator using four-port scattering matrix," *IEEE Transactions on Microwave Theory and Techniques*, vol. 30, no. 10, pp. 1801–1804, Oct. 1982.

[11] R. R. Carreira, J. J. Barroso, and J. E. B. Oliveira, "Mitigation of chromatic dispersion in fiber-optic link using dual-drive mach-zehnder modulator and heterodyne detection technique," in *2019 SBMO/IEEE MTT-S International Microwave and Optoelectronics Conference (IMOC)*. IEEE, Nov. 2019.

[12] K. Xu, J. Dai, R. Duan, Y. Dai, Y. Li, J. Wu, and J. Lin, "Instantaneous microwave frequency measurement based on phase-modulated links with interferometric detection," *IEEE Photonics Technology Letters*, vol. 23, no. 18, pp. 1328–1330, Sep. 2011.